Spatial Reuse in Underwater Acoustic Networks using RTS/CTS MAC Protocols

University of Massachusetts Amherst, Dept. of Computer Science Technical Report UM-CS-2010-045

Jim Partan*†, Jim Kurose*, Brian Neil Levine*, James Preisig†
*University of Massachusetts, Amherst, Dept. of Computer Science
partan@cs.umass.edu, kurose@cs.umass.edu, brian@cs.umass.edu
†Woods Hole Oceanographic Institution, Dept. of Applied Ocean Physics and Engineering
jpartan@whoi.edu, jpreisig@whoi.edu

***Abstract*—Using analytic models and simulation results, we examine spatial reuse and the effectiveness of RTS/CTS MAC protocols in underwater acoustic networks. We are not looking at the question of network throughput, which is affected mostly by propagation delay, but rather the protocol's ability to prevent collisions.**

RTS/CTS-based collision-avoidance protocols require successful detection of the handshake packets in order to be effective. This criterion leads to an RTS/CTS effectiveness metric which depends upon channel characteristics such as spreading loss, attenuation, and ambient noise, as well as communication parameters such as the detection threshold and type of modulation.

The relatively low spreading losses in underwater acoustic channels allows increased interference from distant interferers, which reduces the effectiveness of collision-avoidance protocols. This in turn reduces spatial reuse and network goodput, and increases power consumption. A competing channel effect, however, is the frequency-dependent attenuation. The attenuation strongly suppresses distant interferers, improving the effectiveness of collision-avoidance protocols. A third channel effect is frequency-dependent ambient noise, which in turn reduces effectiveness for links consisting of widely separated nodes. The RTS/CTS effectiveness generally decreases with decreasing acoustic frequency.

In terms of communication parameters, RTS/CTS effectiveness and spatial reuse decrease with increasing detection threshold. This implies that modulation techniques which work with low-SINR packet detectors, such as low-bitrate FH-FSK, will have good spatial reuse. Modulation techniques such as high-bitrate PSK, however, require higher detection thresholds, and will have reduced collision-avoidance effectiveness.

We present analytic, numerical, and simulated results detailing how each of the major characteristics of the physical channel and physical layer affect the RTS/CTS effectiveness.

I. Introduction

Underwater wireless sensor networks for oceanographic applications rely on underwater acoustic communication at the physical layer. Underwater acoustic communication channels have a number of physical differences from terrestrial radio communication channels, including speed of propagation, spreading loss model, as well as frequency-dependent attenuation and ambient noise. Previous work on RTS/CTS-based MAC protocols in the domain of underwater acoustic networks (UANs) has mostly focused on propagation delay issues. While RTS/CTS-based protocols are usually relatively inefficient due to large propagation delays [1], [2], they are nevertheless being proposed for underwater acoustic networks, in part due to their practical simplicity [3]–[7].

In this paper, we analyze the effects of spreading losses, frequency-dependent attenuation, and frequency-dependent ambient noise on collision-avoidance protocols derived from MACAW [8], i.e. using RTS/CTS/DATA/ACK handshakes. Specifically, we use analytic results, numerical results, and simulations to evaluate the effectiveness of RTS/CTS-based collision avoidance in UANs. The effectiveness of the collision avoidance protocol determines the degree to which spatial reuse is possible within the network. Previous work on spatial reuse in UANs has dealt with TDMA and FDMA cellular architectures [9], rather than RTS/CTS-based ad hoc networks.

We build on previous work by Xu et al. [10] which argues that for 802.11-based radio networks, packets can cause collisions at ranges significantly larger than the range at which they can be detected. In this case the RTS/CTS handshake cannot prevent all collisions, which reduces spatial reuse, network efficiency, and power efficiency. The range at which interferers can cause collisions depends upon the distance between transmitter and receiver, the packet detection threshold, and the physical channel characteristics.

In UANs, physical waveguide effects in the communications channel reduce spreading losses significantly relative to radio channels. The small spreading loss allows interference from distant nodes. A competing physical effect is from attenuation, which can suppress distant interferers strongly, improving spatial reuse. A third effect is that of ambient noise, which reduces the effectiveness of RTS/CTS collision avoidance for widely-spaced nodes. Aside from spreading, these effects are frequency-dependent, and analyzing spatial reuse in UANs is a complex problem.

Our contributions in this paper include the following:

- We extend Xu et al.'s basic model to a simple channel model for UANs that considers spreading losses only. The properties of UANs invalidate one of their original assumptions, which we fix. The resulting solution suggests that on average, RTS/CTS handshakes begin to lose effectiveness in UANs for node separations of

only 22% of the maximum range, versus about 56% for radio networks, for typical parameters.

- We switch to a more realistic channel model that includes spreading loss, frequency-dependent attenuation, and frequency-dependent ambient noise. We present numerical results for the RTS/CTS effectiveness, and also derive physically based analysis to explain how different communication parameters — including detection threshold, node separation, transmit power, attenuation coefficients, ambient noise power — affect spatial reuse. We find that the strong effects from attenuation improve spatial reuse for most intermediate node separations to approximately the level of collision-avoidance performance in RF networks.
- We hypothesize an mixed-exponent spreading model with different spreading exponents for signal and interference, as an alternative in certain situations to the widely accepted $k \approx 1.5$ spreading model, including when using high-bitrate PSK packets requiring coherent detection. While this model is not experimentally verified, we present a plausible argument supporting it in terms of channel physics and the standard matched-filter detector algorithms commonly used to synchronize high-bitrate PSK packets. In channels in which this hypothesized mixed-exponent spreading model holds, RTS/CTS effectiveness would drop significantly, especially for low frequencies. For instance, at 3 kHz, on average the RTS/CTS handshake would suppress under 10% of potential interferers for all but the smallest node separations.
- We validate the numerical results from our analytical model with a simulator incorporating the channel model, physical layer, and link-layer MAC protocols.

We conclude with a discussion of several possible methods for improving spatial reuse in UANs using RTS/CTS-based MAC protocols.

II. Background

Our contributions extend a basic model of RF MAC-layer behavior by Xu et al. [10] (and Ye et al. [11]). Their study of RTS/CTS-based MAC protocols found that interference from nodes that are out of data communication range can cause collisions; that is, the interference range of transmissions is typically larger than the data range. In this section, we re-state their model and results, and in the next section, we extend the model to account for the physical properties of underwater acoustic communication channels.

Xu et al.'s analysis begins with the simple statement that collision avoidance requires the successful detection of RTS/CTS packets. In other words, it must be that

$$T \leq \text{SINR}, \tag{1}$$

where T is the receiver's detection threshold, and SINR is the signal-to-interference-and-noise ratio at the receiver. Following the notation introduced by Xu et al., let d be the distance between transmitter and receiver. Let r be the distance from receiver to the closest interferer. The simple model analyzed by Xu et al. does not include ambient noise and signal attenuation, reducing SINR to SIR, the signal-to-interference ratio. The RF-based networks they study have a spreading exponent of $k \approx 4$ for a two-ray ground-reflection model [12]. In that case, Equation 1 becomes

$$T \leq \text{SIR} = \frac{Pd^{-k}}{Pr^{-k}} = \left(\frac{r}{d}\right)^k \tag{2}$$

where P is the transmit power for all nodes. Choosing equality in Eq. 2 gives the minimum allowable distance r to the interferer such that the collision-avoidance between source and receiver is successful. Let this minimum allowable distance be denoted by R_i. Defining

$$\gamma = R_i/d \tag{3}$$

gives $\gamma = T^{1/k}$ for this simple channel model. We examine γ in greater detail in the next sections, extending it to a frequency-dependent form for more realistic channel models. We refer to γ as the *interference range ratio*, and it is the fundamental quantity of interest in this paper since it determines the effectiveness of the collision-avoidance protocol. For the simple model in this section, with spreading losses only, γ is a constant, which we denote by $\gamma_o = T^{1/k}$.

Let R_{tx} be the maximum transmission range of all packets such that detection is successful. If $R_i \leq R_{\text{tx}}$, then the CTS packet will reach all potential interferers, and suppress their transmissions. If, however, $R_i > R_{\text{tx}}$, then some interferers will not be suppressed, leading to packet collisions.

The maximum separation of any two communicating nodes is when $d = R_{\text{tx}}$, and so if $\gamma > 1$, then R_i can be greater than R_{tx} for some nodes in the network. In this case, the collision-avoidance protocol is not fully effective. As R_i (or γ) increases, the number of potential interferers increases dramatically, roughly as R_i^2 for a 2-dimensional network deployment. (It is possible for UANs to be 3-dimensional [13], but most applications are in fact 2-dimensional deployments.) While it is well-known that wireless network nodes do not have a circular (or spherical) coverage region [14], this approximation allows the physical analysis in this paper, offering theoretical insight into the protocol performance.

For RF wireless networks, setting $k = 4$ and $T = 10$ dB gives $\gamma_o = 1.8$. Even at this relatively small value of γ_o, Xu et al. and Ye et al. conclude that interference in RF networks can greatly reduce collision-avoidance protocol effectiveness.

Xu et al. also define the RTS/CTS effectiveness, $E_{\text{RTS/CTS}}$, as the fraction of the interference region that is covered by the collision-avoidance RTS/CTS handshake packets. In a 2-dimensional network deployment, assuming uniform node distribution and transmission times, this is a ratio of areas:

$$E_{\text{RTS/CTS}} = \frac{A_{(i \cap \text{RTS/CTS})}}{A_i}, \tag{4}$$

where A_i is the area in which there could be a potential interferer, $A_{\text{RTS/CTS}}$ is the area covered by the RTS/CTS collision avoidance protocol, and $A_{(i \cap \text{RTS/CTS})}$ is the intersection of these regions.

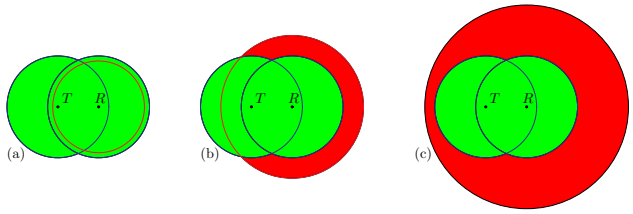

Fig. 1: Three scenarios of interference range: (a) Scenario I, with interference range R_i less than transmission range $R_{\rm tx}$, and all potential interferers suppressed by the RTS/CTS handshake; (b) Scenario IIa, with some of the potential interferers not suppressed by the RTS/CTS handshake (red area); (c) Scenario IIb, with many potential interferers not suppressed (red area).

III. Deriving γ_o for Underwater Acoustic Channels: Spreading-Only Model

To extend the model to underwater acoustic channels, our first challenge is to account for the waveguide effects that result in much lower spreading exponents, often taken as so-called "practical spreading", with $k \approx 1.5$ [7], [15]. For UANs, setting $k = 1.5$ and $T = 10$ dB gives $\gamma_o = 4.6$. Therefore, we see immediately that long-range interference can be a more significant problem in UANs than it is in RF wireless networks, and it is worth investigating this problem in more detail.

While it is easy to simply apply Eq. 2 for a different spreading exponent, applying Eq. 4 to underwater channels is non-trivial as Xu et al.'s analysis made an approximation that does not apply to underwater channels.

A. RTS/CTS Effectiveness

The are three possible scenarios when comparing the distances of the source, receiver, and interferer. They are illustrated in Figure 1 and enumerated here:

- I: $0 < R_i < R_{\rm tx}$: the geographic range of CTS packets covers all potential interferers.
- IIa: $R_{\rm tx} < R_i < R_{\rm tx} + d$: the range of CTS packets covers most of the area from which third parties can interfere.
- IIb: $R_{\rm tx} + d < R_i$: The range of CTS packets covers a small fraction of the area from which third parties can interfere.

Note that in RF networks with a detection threshold of $T < 12$ dB, Scenario IIb does not occur, and so it is not analyzed in previous work. Xu et al. and Ye et al. use an approximation for $A_{(i \cap \text{RTS/CTS})}$ based on an idealized circular geometry for wireless range that only is valid for Scenario IIa. When Scenario IIb does occur, as it will for most underwater networks, that approximation will lead to a discontinuity in $E_{\rm RTS/CTS}$.

We derive a new calculation of $A_{(i \cap \text{RTS/CTS})}$, exact in this idealized case of circular transmission ranges, that is valid for all three scenarios, shown in the Appendix. For the simplified channel model (i.e., without considering attenuation or ambient noise), we use the results from the Appendix to plot $E_{\rm RTS/CTS}$ for RF and underwater acoustic networks in Figure 2. We set the detection threshold

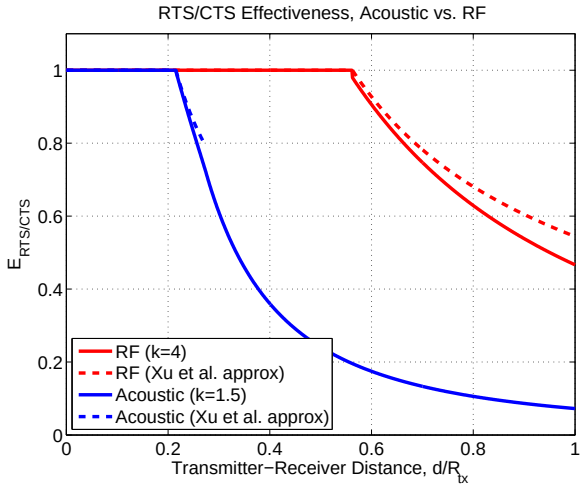

Fig. 2: RTS/CTS effectiveness in underwater networks is hurt significantly by long-range interference. The dotted lines use the approximation in [10] and [11], and the solid lines use the equations derived in the appendix. The case with $T = 10$ dB and without attenuation and ambient noise is plotted.

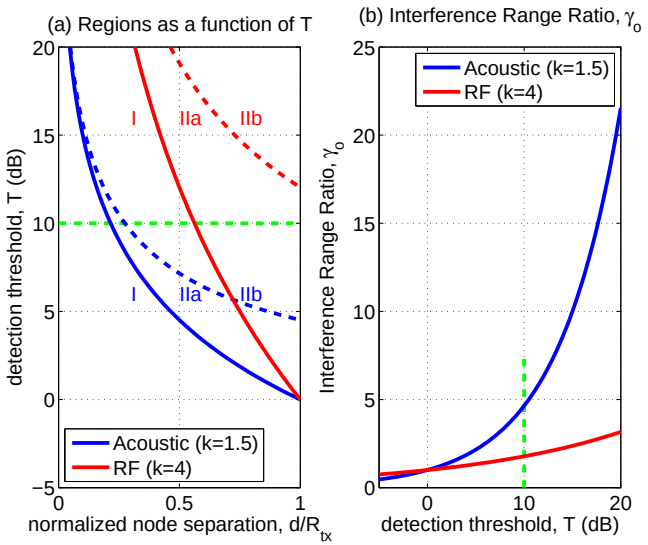

Fig. 3: (a) Regions for Scenarios I, IIa, and IIb as a function of detection threshold (T on vertical axis). See Figure 1 and Table I for scenario definitions. (b) Interference range ratio γ_o as a function of detection threshold T. In both (a) and (b), the green dashed line indicates $T = 10$ dB; the case for no ambient noise and no attenuation is plotted.

$T = 10$ dB, and use spreading exponents of $k = 4$ and $k = 1.5$, respectively. For these same conditions, Table I shows the normalized node separations $d/R_{\rm tx}$ for which each of the three scenarios applies. In Figure 2, the dotted-line shows the values obtained by Xu et al.'s approximation, and the solid lines are the result of our exact calculation. Xu et al.'s results for acoustic networks end quickly as their assumptions become invalid and the calculation becomes discontinuous.

Table I and Figure 2 replicate Xu et al.'s results, and extend them to a simple underwater acoustic channel model, with spreading losses only. In an RF network, when the

Scenario	Interval	Normalized	$E_{\mathrm{RTS/CTS}}$	**RF** $(k = 4)$	**Acoustic** $(k = 1.5)$
I (Fig 1a)	$0 < R_i < R_{\mathrm{tx}}$	$0 < \frac{d}{R_{\mathrm{tx}}} < \frac{1}{\gamma}$	1	$0.000 < \frac{d}{R_{\mathrm{tx}}} < 0.562$	$0.000 < \frac{d}{R_{\mathrm{tx}}} < 0.215$
IIa (Fig 1b)	$R_{\mathrm{tx}} < R_i < R_{\mathrm{tx}} + d$	$\frac{1}{\gamma} < \frac{d}{R_{\mathrm{tx}}} < \min(\frac{1}{\gamma-1}, 1)$	$\frac{A_{(i \cap \mathrm{RTS/CTS})}}{A_i}$	$0.562 < \frac{d}{R_{\mathrm{tx}}} < 1.000$	$0.215 < \frac{d}{R_{\mathrm{tx}}} < 0.275$
IIb (Fig 1c)	$R_{\mathrm{tx}} + d < R_i$	$\frac{1}{\gamma-1} < \frac{d}{R_{\mathrm{tx}}} < 1$	$\frac{A_{\mathrm{RTS/CTS}}}{A_i}$		$0.275 < \frac{d}{R_{\mathrm{tx}}} < 1.000$

TABLE I: The three regions for d/R_{tx}. Note that $d/R_{\mathrm{tx}} < 1$. Columns 5 and 6 are for $T = 10$ dB, with no attenuation or ambient noise, i.e. $\gamma_o = 1.8$ for RF and $\gamma_o = 4.6$ for UANs.

source/receiver pair are in Scenario I (i.e., when d/R_{tx} is less than about 56% for $T = 10$ dB) then the RTS/CTS collision avoidance protocol is fully effective — all potential interferers are suppressed. For larger source-to-receiver separations, the RTS/CTS protocol becomes increasingly ineffective. For RF networks with detection threshold $T < 12$ dB, the network will always be in Scenarios I or IIa, as Figure 3a illustrates graphically.

For UANs, however, with a typical spreading loss of $k = 1.5$ and detection threshold of $T = 10$ dB, then the RTS/CTS collision avoidance protocol starts losing effectiveness when d/R_{tx} is larger than about 22%. The collision-free region therefore covers less than 5% of the area within the maximum transmission range.

B. Effects of Detection Threshold on γ_o

Figure 3b show how the interference range, R_i, increases sharply with an increasing detection threshold, T in this model. For efficient RTS/CTS MAC protocols, it is therefore *important to minimize the packet detection threshold.*

Incoherent detection methods, such as detecting the start of the packet by detecting coded sequences of frequency-hopped FSK signals (FH-FSK), generally have low detection thresholds, which can be 3 dB or less [16]. These low detection thresholds will allow significant spatial reuse when using robust, low bitrate modulation and coding techniques for which timing synchronization requirements can be supported by FH-FSK or other low-SINR detection techniques.

Packets with higher bitrates generally use PSK modulation, and the detector needs to detect the start of the packet with higher time resolution than FH-FSK methods can provide [17]. Coherent detection methods, such as matched-filter detectors, typically require detection thresholds of around 10 dB. Therefore, with the higher detection threshold required for packets with higher bitrates, γ_o increases significantly as shown in Figure 3b, reducing spatial reuse in the network.

IV. Extending the Interference Model

In this section, we introduce a more realistic underwater acoustic channel model, incorporating attenuation and ambient noise. In RF communications, which occur over much shorter ranges typically (e.g., 300 m), attenuation is usually neglected in models. Similarly, RF noise is qualitatively different; often assumed to be electrical noise within the receiver, it is similarly neglected. In underwater networks, however, ambient noise from ships, wind-driven waves, rain, shrimp, etc. is a fundamental part of the natural acoustic environment and cannot be neglected.

Following Stojanovic [15], we use Thorp's expression[1] for the frequency-dependent acoustic energy attenuation coefficient, $\alpha(f)$, which is generally expressed in dB per unit distance. To model ambient noise power, $\sigma_N(f)$, we use the empirical power spectral density (PSD) from Stojanovic [15], parameterized by a shipping factor of 0.5 and wind speed of 3 m/s. We integrate this PSD across a bandwidth of $1/3$ of the center frequency, which is typical of acoustic transducers used in UANs.

For our spreading model, at first we again use the "practical spreading" model, with a spreading exponent of $k = 1.5$. In Section V, we propose an alternate physically based spreading model that has lower spreading losses for interfering signals and higher spreading losses for signals that require detection.

We do not use transmit power control, and we use a fixed transmit power of 185 dB re:1μPa@1m, a typical value for underwater acoustic modems.

A. Calculating $\gamma(f, d)$

By including attenuation and ambient noise, γ is no longer a constant. In this extended model, $\gamma(f, d)$ is a function of frequency f and source-receiver separation d. We start with the condition for detection $T \leq \mathrm{SINR}$ (Eq. 1). This expression achieves equality for the minimum allowable SINR for detection, which occurs at the minimum allowable interferer range, R_i:

$$T = \mathrm{SINR} = \frac{P_s\ S(d,k)\ A(f,d)}{P_i\ S(R_i,k)\ A(f,R_i) + \sigma_N(f)} \qquad (5)$$

In this expression, the transmit powers for source and interferer are P_s and P_i, respectively. In all plots in this section, we set $P_s = P_i$. The spreading loss factor is $S(r,k) = (r/r_o)^{-k}$, where r_o is a reference distance, typically taken as $r_o = 1$ m. The attenuation factor is $A(f,r) = 10^{-\alpha(f)r/10}$. The ambient noise power at the receiver is $\sigma_N(f)$.

SINR is a critical metric for this paper, but using it also has a number of practical complications, explored by Son et al. [19]. These complications include the facts

[1]Marsh and Schulkin [18] offer an alternative to Thorp's expression that can be more accurate for frequencies above about 3 kHz, with somewhat lower attenuation, but we leave an exploration of the differences for future work.

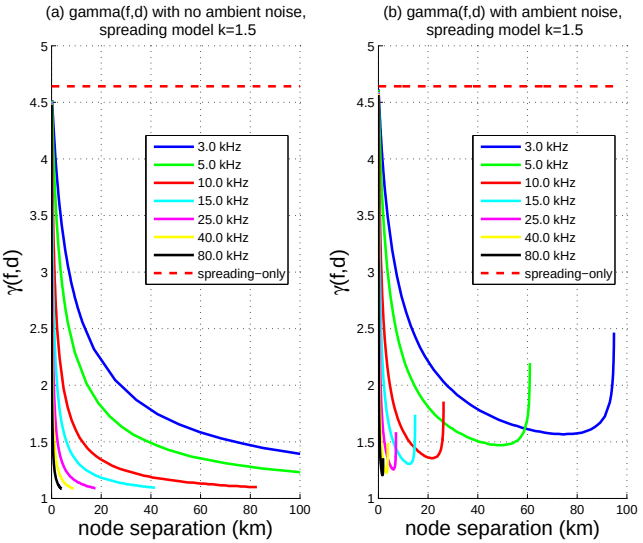

Fig. 4: Numerical solutions for $\gamma(f,d)$ for the spreading model $k = 1.5$, with attenuation, for several frequencies. (a) is without ambient noise; (b) includes ambient noise. The dashed lines show comparisons with the case of spreading losses only.

that interference from multiple interferers does not add linearly, there is hardware variation among receivers, and even that adding interferers can increase the effective detection threshold of the detection algorithm [19]. For the purposes of this paper, however, we are just considering a single interferer at range R_i and idealized receivers.

Returning to our derivation, since $R_i = \gamma\, d$, then from Equation 5,

$$\gamma^{-k}\,(A(f,d))^{(\gamma-1)} = \frac{P_s}{P_i T} - \frac{\sigma_N(f)}{P_i\, S(d,k)\, A(f,d)} \qquad (6)$$

In general, there is no closed-form solution of Equation 6 for $\gamma(f,d)$. We can, however, solve this equation (or its equivalent, taking logarithms) numerically, and we discuss the results below.

B. Effects on $\gamma(f,d)$ of Ambient Noise and Attenuation

Attenuation and ambient noise add strong frequency-dependent effects to the interference range ratio, $\gamma(f,d) = R_i/d$. Figure 4 shows $\gamma(f,d)$ for typical acoustic communication frequencies ranging from 3 kHz to 80 kHz for a spreading exponent of $k = 1.5$. Figure 4a shows $\gamma(f,d)$ *without* ambient noise, while Figure 4b shows $\gamma(f,d)$ *with* ambient noise, to help distinguish the effect of each. We examine the results in three parts: small, intermediate, and large node separations.

For small node separations, spreading losses dominate. In that case, attenuation and ambient noise can be neglected, and γ approaches γ_o. This can be seen in both Figures 4a and 4b.

For intermediate node separations, attenuation losses dominate and largely determine the shape of the $\gamma(f,d)$ curves in Figure 4. If we neglect ambient noise (letting $\sigma_N(f) = 0$), and focus on the intermediate separation distances, we can ignore the spreading term γ^{-k} in Eq. 6. In that case, intermediate node separations can be described as

$$\gamma(f,d) \approx 1 + \left(\frac{10\log_{10}(T)}{\alpha(f)}\right)\frac{1}{d}. \qquad (7)$$

Spreading losses are polynomial in range, whereas attenuation losses are exponential in range (i.e., for range r, spreading losses scale as r^{-k}, and attenuation losses scale as $10^{-\alpha(f)r/10}$). For all but the smallest node separations, therefore, this intermediate case applies, and $\gamma(f,d)$ scales as $1/d$ in this region.

When node separations are large and approach the maximum transmission range, ambient noise starts to affect $\gamma(f,d)$ significantly. This can be seen by comparing Figures 4a and 4b.

The maximum transmission range is when no interferers are present, so the signal-to-noise ratio equals the detection threshold, i.e., $T = \text{SNR}$. In that case, R_{tx} is the numerical solution of Eq. 5, with $P_i = 0$:

$$\left(\frac{R_{\text{tx}}}{r_o}\right)^{-k} A(f,R_{\text{tx}}) = \frac{T\,\sigma_N(f)}{P_s}. \qquad (8)$$

For node separations that approach the maximum transmission range, even a small amount of interference will prevent detection. As the node separation approaches the maximum transmission range, the minimum allowable distance from the receiver to an interferer for successful detection approaches infinity. So, when ambient noise is included in the model, $\gamma(f,d)$ approaches infinity as the node separation approaches the maximum transmission range.

One way to avoid this problem is to set the UAN's routing tables so that packets are not routed on links whose node separation approaches the maximum transmission range. This is a caveat to the general idea that one should route over long hops in a wireless network [20].

The competing effects of attenuation and ambient noise lead to the minimum in $\gamma(f,d)$ apparent in Figure 4b.

C. RTS/CTS Effectiveness with Attenuation and Ambient Noise

The RTS/CTS MAC protocol can avoid all collisions only if all potential interferers can detect the RTS or CTS successfully. Since interference occurs at the receiver, it is especially important that a potential interferer can detect the CTS packet. Section II introduces the RTS/CTS effectiveness metric, $E_{\text{RTS/CTS}}$. In Table I, we have expressions for $E_{\text{RTS/CTS}}$ (column 4) and the regimes of node separations over which each expression applies (column 1). Given a node separation d, we can calculate the interference range, $R_i = \gamma(f,d)\,d$, where $\gamma(f,d)$ is the numerical solution of Equation 6, plotted in Figure 4. From Equation 8, we can calculate the maximum transmission range, R_{tx}.

In the expressions for $E_{\text{RTS/CTS}}$, the terms $A_i = \pi R_i^2 = \pi\gamma^2 d^2$, and both $A_{\text{RTS/CTS}}$ and $A_{(i\cap\text{RTS/CTS})}$, are derived analytically in the Appendix. We can then calculate $E_{\text{RTS/CTS}}$ for a given frequency f as a function

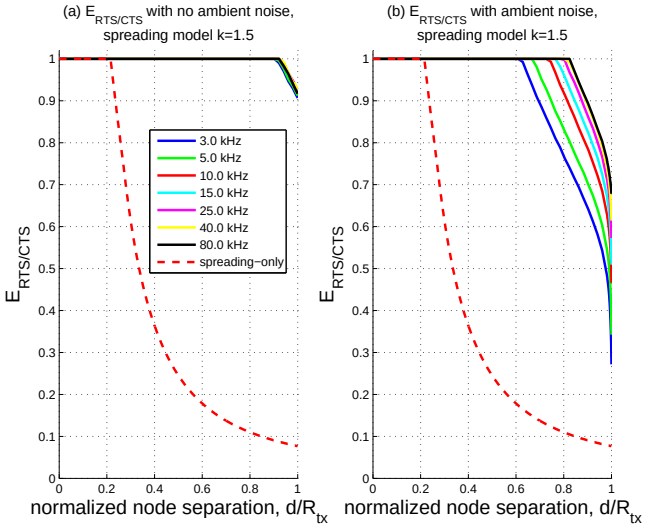

Fig. 5: $E_{\mathrm{RTS/CTS}}$, calculated with Table I and $\gamma(f,d)$ from Figure 4, for several frequencies, with spreading and attenuation losses. (a) is without ambient noise, while (b) includes ambient noise. The red dashed lines show comparisons with the case of spreading losses only. The plot legend/key is the same for both (a) and (b).

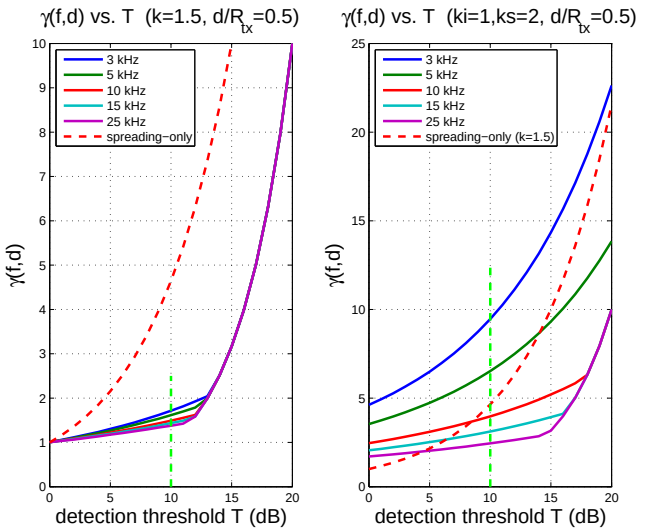

Fig. 6: $\gamma(f,d)$ as a function of detection threshold T for several frequencies, with attenuation and ambient noise. The plots are for a normalized node separation of $d/R_{\mathrm{tx}} = 0.5$. The green dashed line marks the case $T = 10$ dB. The dashed red line shows the spreading-only case, as in Figure 3b. (a) Spreading exponent $k = 1.5$. (b) Alternate spreading model from Section V. Note different vertical scales.

of node separation d, up to the maximum node separation, R_{tx}. This function is plotted in Figure 5.

Since the attenuation reduces $\gamma(f,d)$ compared with the spreading-only case, $E_{\mathrm{RTS/CTS}}$ is improved compared with the spreading-only case, as shown in Figure 5. When ambient noise is included, $E_{\mathrm{RTS/CTS}}$ drops for node separations which approach the maximum transmission range, shown in Figure 5b. Effectiveness is lower for lower acoustic frequencies.

D. Effects of Detection Threshold on $\gamma(f,d)$

In Section III-B and Figure 3b, we show the effects of detection threshold T on γ_o in the spreading-only channel model. With attenuation and ambient noise, the results are similar: $\gamma(f,d)$ increases rapidly with increasing detection threshold. Figure 6 plots $\gamma(f,d)$ as a function of detection threshold for several frequencies. Figure 6a shows the case with spreading exponent $k = 1.5$, and Figure 6b shows the case with the alternate spreading model introduced in Section V.

V. A Mixed-Exponent Spreading Model

The practical spreading approximation of $k \approx 1.5$ is a widely accepted spreading model for point-to-point underwater communication links [15]. Spreading models for underwater acoustic communications have been based mostly on detecting signals on point-to-point links. With UANs, interference becomes a significant concern. As we discuss below, in the case of detecting high-bitrate packets in a UAN, an alternate spreading model with different spreading exponents for signal and interference, may be more appropriate than the practical spreading model. This has not yet been verified. We present results showing that, if the mixed-exponent spreading model is in fact valid, the RTS/CTS effectiveness can be very low, especially for UANs transmitting on low frequencies.

The origin of the $k \approx 1.5$ spreading model draws from the basic physics. Energy from a point source transmitter in an idealized channel of very deep, uniformly mixed water will experience spherical spreading, such that $k \approx 2$. In most situations, however, multipath effects from either shallow water reflections or a deep-water refractive sound channel will lead to waveguide effects reducing the effective spreading exponent. In the idealized case of shallow water with a perfectly reflecting surface and bottom, the *incoherent* sum of the energy from a point source will experience cylindrical spreading, such that $k \approx 1$, at large ranges relative to the water depth. The practical spreading model with $k \approx 1.5$ is a combination of these two regimes.

A. Signal and Interference Spreading

In our hypothesized model, we assign separate spreading exponents to signal and interference. The basic intuition for the difference is that receivers process signal and interference differently when detecting the start of a packet (aside from multiuser receivers, which traditionally have had high computational complexity [21]). This difference may effectively increase the spreading exponent for signals and decrease it for interference.

Signal spreading. For FH-FSK communication, which typically has low bitrates, packet detectors are incoherent energy detectors, generally detecting on FH-FSK tone patterns, with low time resolution. Higher bitrates generally require PSK modulation or OFDM. PSK requires a precise time synchronization on the start-time of the packet, while OFDM requires precise frequency synchronization [22].

For PSK packets, *coherent* detectors, such as matched-filter detectors, detect on a known signal at the start of the packet, and they provide the precise timing measurements required for these high-bitrate packets. This initial detection is before the receiver's adaptive equalizer has been trained, and so the initial detection typically detects on just a *single* multipath arrival. In other words, when detecting the start of high-bitrate data packets, the signal's effective spreading loss is the spreading loss experienced by a single multipath arrival, and accordingly $k_s \approx 2$ (here, the subscript s is for signal).

Beyond a certain range, however, separate multipath arrivals become unresolvable, and they *coherently* combine in the received signal. This is the region in which the signal spreading transitions from a spherical-spreading regime ($k_s \approx 2$) to a cylindrical-spreading regime ($k_s \approx 1$). This range depends upon the bandwidth of the signal (increasing with bandwidth), and also upon the water depth (increasing with depth).

With an OFDM system, the overall bandwidth is divided into many small sub-bands, in contrast to a single band for a PSK system. Therefore, for each sub-band, the range at which k_s transitions from spherical to cylindrical spreading would be smaller with OFDM compared with PSK, if the mixed-exponent spreading model is valid. This would improve the RTS/CTS effectiveness for OFDM-based systems relative to PSK-based systems.

Detection generally is the limiting factor for most packets, since the error-correction coding can be designed appropriately so that essentially all detected packets can be decoded successfully.

Interference spreading. The interference, however, combines *incoherently*, and energy from *all* multipath paths is combined. A physically based model for the interference spreading loss is

$$S(r, w_d, k_i) = \begin{cases} \left(\frac{r}{r_o}\right)^{-2} & r < w_d \\ \left(\frac{w_d}{r_o}\right)^{-2} \left(\frac{r}{w_d}\right)^{-k_i} & r \geq w_d \end{cases} \quad (9)$$

where r is the range from transmitter to receiver (ignoring slant range for the time being), w_d is the water depth, r_o is a reference distance (typically 1 m), and $k_i \approx 1$ is the spreading exponent for interference for ranges larger than the water depth. Similarly, we also use this model for signal spreading loss, $S(r, w_d, k_s)$, with the complication that k_s will transition from $k_s \approx 2$ to $k_s \approx 1$ beyond a certain range (we have omitted this transition in our numerical results in this section).

B. Implications for $\gamma(f, d)$ and $E_{\mathrm{RTS/CTS}}$

To use the interference spreading model from Eq. 9, we adjust Eq. 5 slightly.

$$T = \mathrm{SINR} = \frac{P_s \; S(d, w_d, k_s) \; A(f, d)}{P_i \; S(R_i, w_d, k_i) \; A(f, R_i) + \sigma_N(f)} \quad (10)$$

We can then numerically solve for $\gamma(f, d)$ as before.

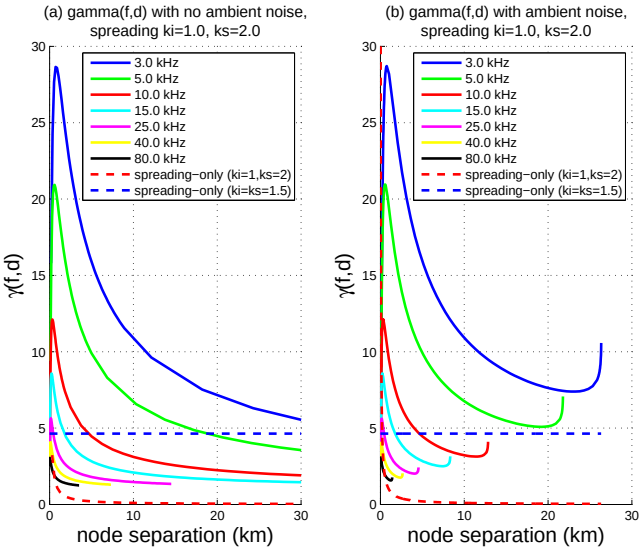

Fig. 7: Numerical solutions for $\gamma(f, d)$ for the spreading model $k_i = 1$, $k_s = 2$, with attenuation, for several frequencies. (a) is without ambient noise; (b) includes ambient noise.

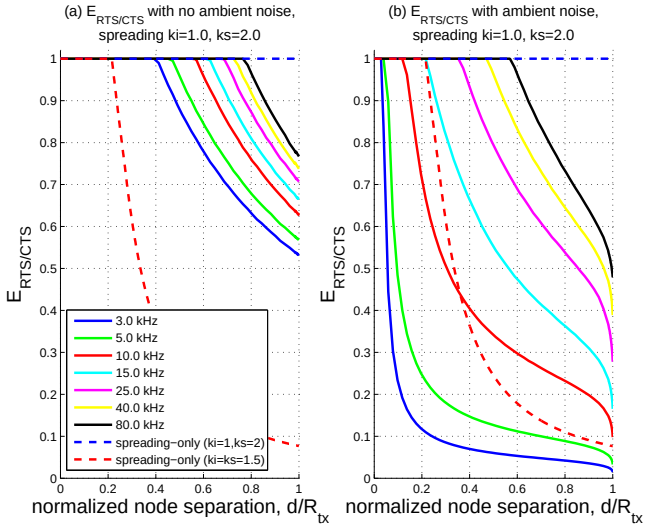

Fig. 8: $E_{\mathrm{RTS/CTS}}$, calculated with Table I and $\gamma(f, d)$ from Figure 7, for several frequencies, with spreading and attenuation losses. (a) is without ambient noise, while (b) includes ambient noise. The dashed lines show comparisons with the case of spreading losses only: the $k = 1.5$ spreading model in red dashes, $k_i = 1$, $k_s = 2$ in blue dashes (which has perfect RTS/CTS efficiency when attenuation losses are not included). The plot legend/key is the same for both (a) and (b).

The water depth now appears explicitly in the spreading model. For the results in Figures 7 and 8, we use a shallow-water environment of $w_d = 100$ m, since shallow water is often the situation of most interest for littoral military operations as well as coastal environmental monitoring.

The notable differences between Figures 4 and 7 are that there now is a maximum $\gamma(f, d)$ value for small node separations, and that maximum can be much larger than the $\gamma(f, d)$ values for $k_i = k_s = 1.5$. For large node separations, Figures 4 and 7 are qualitatively similar, though in Figure 7, $\gamma(f, d)$ remains quite large even for large node separations.

We can provide an intuitive physical explanation for the maximum in $\gamma(f,d)$, deriving its location and amplitude in terms of physical parameters of the communications channel.

For small node separations, we can ignore ambient noise. Then with the alternate spreading model, Eq. 6 from the previous section becomes

$$\gamma^{-k_i}\,(A(f,d))^{\gamma-1} = \frac{P_s}{P_i T}\,\left(\frac{d}{w_d}\right)^{(k_i-k_s)} \tag{11}$$

For very small node separations, we can also ignore attenuation losses. In the case of very small node separations, setting $k_i = 1$ and $k_s = 2$, we have

$$\gamma \approx \left(\frac{P_i T}{P_s}\,\frac{d}{w_d}\right). \tag{12}$$

Therefore, for very small node separations, $\gamma(f,d)$ increases approximately linearly with node separation, up to a maximum. This maximum occurs when spreading losses balance with attenuation losses. When the attenuation losses dominate, then $\gamma(f,d)$ drops sharply, as explained in the previous section.

To find the maximum, $\gamma_{\max} = \gamma(f, d_{\max})$, we differentiate Eq. 11 with respect to d, and set the derivative of γ equal to zero. From Figure 7 we can see that $\gamma_{\max}$ is relatively large (so for this analytical derivation we approximate $\gamma_{\max} \gg 1$), and the maximum occurs for small $d_{\max}$ (and so $A(f, d_{\max}) \approx 1$). Setting $k_i = 1$, $k_s = 2$, these approximations give

$$d_{\max} \approx \beta\,\left(\frac{P_s}{T P_i}\,\frac{w_d}{\alpha(f)}\right)^{1/2}, \tag{13}$$

where $\beta = (10\log_{10}(\exp(1)))^{1/2}$. Plugging this value for $d_{\max}$ back into Eq. 12 gives an overestimate for $\gamma_{\max}$, since $\gamma(f,d)$ is convex in the neighborhood of its maximum:

$$\gamma_{\max} \approx \beta\,\left(\frac{T P_i}{P_s}\,\frac{1}{w_d\,\alpha(f)}\right)^{1/2}. \tag{14}$$

This result gives an intuition for which physical parameters control the amplitude and location of the maximum in $\gamma(f,d)$.

With this mixed-exponent spreading model, $\gamma(f,d)$ obtains much higher values than it does with the practical spreading model. As a result, we see significantly lower RTS/CTS efficiency, as shown in Figure 8b. For low frequencies, the MAC efficiency is particularly low. The plot shows center frequencies as low as 3 kHz. These are realistic frequencies for actual UANs; for instance, the PLUSNet deployment [23] includes a long-range channel with a center frequency of about 3 kHz.

One implication of Figure 8b is that for multiband UANs [4], [23], different bands might use different MAC protocols; for certain deployments, RTS/CTS effectiveness might be considered acceptable on a high-frequency band (which would have small node separations, reducing the propagation delays), but unacceptable for the low-frequency bands, with long node separations and the double penalty of low $E_{\mathrm{RTS/CTS}}$ due to spreading effects, and low throughput due to propagation delays.

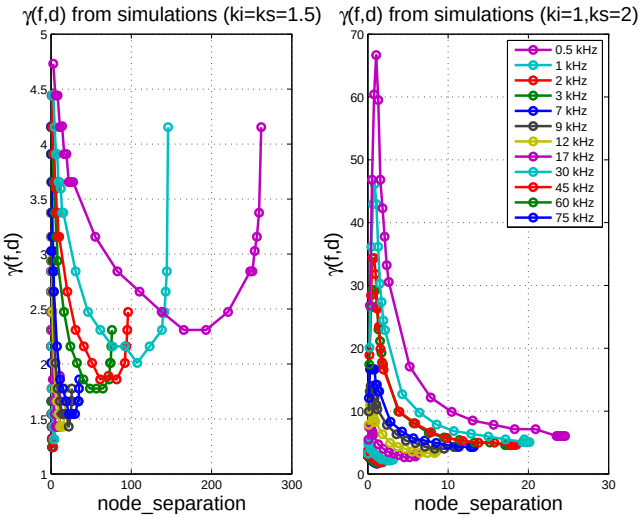

Fig. 9: Simulation results for $\gamma(f,d)$. The plot's legend holds for both the left-hand and right-hand plots. Note the very different scales on the vertical axis for the two plots. C.f., Figs. 4b and 7b, respectively.

There is no standard accepted model for underwater communications channels [24], though our choices for $k = 1.5$ spreading, attenuation, and ambient noise are consistent with the literature. Most work in underwater acoustic communication has focused on point-to-point links rather than networks, and it might be the case that spreading models need to be re-visited fully, at a minimum with a modal simulation [18], and perhaps with an SINR measurement study analogous to Son et al. [19]. Such a study would help determine the validity of the mixed-exponent spreading model, values for the spreading exponents k_i and k_s, and values for the range where k_s transitions from spherical to cylindrical spreading.

VI. Simulation Results for the Interference Range

To validate our numerical results, we implemented a simulator that includes a physical channel model, a simulated physical layer, and link-layer MAC protocol for each node.

The main goal of the simulator is to calculate $\gamma(f,d)$, and therefore the key measurement is the interference range, R_i. By definition, any interferer within the interference range will prevent packet detection, preventing the RTS/CTS handshake from completing.

To measure the minimum allowable interference range, we ran simulations with three nodes. Node 1 and node 2 were a source and receiver pair. They attempted to complete RTS/CTS/DATA/ACK data transfer handshakes, with node 2 receiving the DATA packet. The third node was placed co-linearly with the first two nodes, with the receiver node in the center. Node 3 transmitted an interfering data packet with a duration equal to the length of the simulation.

The parameters for a simulation run include:

- The frequency f of the transmitted data and interference packets. We varied f from 3 kHz to 75 kHz, closely matching the analytical plots.
- The spreading model. Using Equation 9, in one group of runs, we set $k_s = k_i = 1.5$; in the second, we set $k_s = 2.0$ and $k_i = 1.0$.
- The separation distance d of the source and receiver pair (labeled *node separation* on the x-axis)
- The distance r between the interfering node and receiver.
- Communication channel parameters such as detection threshold and transmit power, as in Section IV.

In addition to spreading, the physical model in the simulation includes attenuation and ambient noise. Attenuation is simulated according to Thorp's expression, and we parameterize noise by the same values as in Section IV, using the empirical PSD in Stojanovic [15].

For each frequency f and source-receiver separation d, we ran simulations for a range of receiver-interferer separations r. The last value of r for which the RTS/CTS/DATA/ACK transaction failed gives an estimate of the minimum value of γ, i.e. $\hat{\gamma}_{\min} = r(\text{last fail})/d$, and similarly the first value of r for which the RTS/CTS/DATA/ACK transaction succeeded gives an estimate of the maximum value of γ, namely $\hat{\gamma}_{\max} = r(\text{first success})/d$. These estimates can be iterated with finer resolution in receiver-interferer separation to achieve tighter tolerances on the estimates of $\gamma(f, d)$.

The results plotted in Figure 9a should be compared against Figure 4b. Figure 9b should be compared against Figure 7b. Both simulation results agree well with the numerical results, and match most of the behavior of the numerical curves. The numerical results for 3 kHz are plotted in Figure 9 to allow comparison with the simulations. We are double-checking our simulator for a potential bug related to maximum transmission ranges, R_{tx}. The maximum transmission range appears to be too small in Figure 9a, and in Figure 9b, only the results for frequencies above 9 kHz exhibit the expected increase in $\gamma(f, d)$ as the node separation approaches the maximum transmission range.

VII. Discussion: Improving Spatial Reuse

The main approaches to improving spatial reuse primarily center on increasing the range of the RTS/CTS handshake. While extending the range of the RTS suppresses other nodes needlessly, a CTS control packet with range equal to the interference range would suppress only potential interferers.

Successful detection is usually the limiting factor for the range of a packet when the error-correcting coding is designed appropriately. To increase the range of a packet with a fixed detection threshold T, we need to increase the SINR at the receiver for the start-of-packet signal. This is usually done by increasing the transmitter power or by increasing the time duration of the signal. Alternately, the frequency band of the packet might be shifted, either to a band with less attenuation (lower frequencies) or to a band with less ambient noise (generally higher frequencies). At higher frequencies of about 40kHz, typical transducer bandwidths (with quality factor $Q \approx 3$) are wide enough to effectively allow a shorter-range channel (for data and RTS) and a longer-range channel (for CTS) with a single transducer, which might be a future possibility.

In extending the range of the CTS signal, the only information that needs to be transmitted to potential interferers is the single bit that a reception is about to occur within their interference range. The interferers do not necessarily need to decode any other information from the CTS header. This might lend itself to a very practical implementation for existing acoustic modems: right before transmitting a CTS packet, transmit a signal with high coding gain (and hence longer range). Any node detecting the CTS signal would enter a quiet backoff state, just as if it had received the CTS packet itself. This would not require any changes to the existing hardware, and would not change either the transmit power or the frequency band.

An additional approach to this problem would be to implement transmitter power control. Transmitter power control is not simple to implement in an energy-efficient manner, however. Underwater modems are very power-constrained, and transmitting uses a lot more power than receiving. Power amplifiers are often high-efficiency, nonlinear Class-D amplifiers that have a fixed output level. Nevertheless, transmit power control can be implemented by using a few discrete fixed output levels, and this would reduce the spatial reuse problems significantly.

VIII. Conclusion

Our analytic models and simulation results demonstrate that RTS/CTS efficiency in UANs is subject to frequency-dependent effects and long-range interference, and not simply acoustic propagation delays. We have provided a closed form solution for γ_0 that is valid for a simple model of acoustic networks, as well as RF networks. We then extended the results to a more realistic channel model that includes ambient noise and attenuation, and presented a numerical solution to $\gamma(f, d)$. Our results show, for the practical spreading model, that both acoustic networks and RF networks have similar performance predictions, despite dramatically different channel models. In both cases, RTS/CTS effectiveness can drop to between 50%–90% for source and receiver separated by more than about two-thirds of the signal range, depending on the frequency in the underwater acoustic case.

We also study the effects of using an alternative physically based spreading model that distinguishes between signals which are coherently detected and interference which is typically incoherently processed. Under such a mixed spreading model, we predict that RTS/CTS effectiveness drops significantly. For example, for the 3 kHz deployment of PLUSNet, RTS/CTS effectiveness would quickly drop to 10% after source and receiver were separated by only 20% of signal range. Finally, we validated our analytical models using a physical simulation and found they matched quantitatively. While several aspects of this problem require closer evaluation from empirical measurements, we believe the results of our models and simulation provide important

insight into the characteristics of interference and RTS/CTS efficiency in underwater networks.

REFERENCES

[1] J. Heidemann, W. Ye, J. Wills, A. Syed, and Y. Li, "Research Challenges and Applications for Underwater Sensor Networking," in *Proc. IEEE Wireless Communications and Networking Conf.*, 2006.

[2] I. F. Akyildiz, D. Pompili, and T. Melodia, "Challenges for efficient communication in underwater acoustic sensor networks," *SIGBED Rev.*, vol. 1, no. 2, pp. 3–8, 2004.

[3] X. Guo, M. R. Frater, and M. J. Ryan, "Design of a Propagation-delay-tolerant MAC Protocol for Underwater Acoustic Sensor Networks," *IEEE Journal of Oceanic Engineering (to appear)*, 2009.

[4] S. Shahabudeen, M. Chitre, and M. Motani, "A multi-channel MAC protocol for AUV networks," in *Proc. IEEE Oceans Europe*, 2007.

[5] M. Molins and M. Stojanovic, "Slotted FAMA: A MAC Protocol for Underwater Acoustic Networks," in *Proc. IEEE OCEANS Conf.*, 2006.

[6] B. Peleato and M. Stojanovic, "A MAC protocol for ad hoc underwater acoustic sensor networks," in *Proc. Workshop on Underwater networks (WUWNet)*, 2006, pp. 113–115.

[7] E. Sözer, M. Stojanovic, and J. Proakis, "Underwater Acoustic Networks," *IEEE Journal of Oceanic Engineering*, vol. 25, no. 1, pp. 72–83, Jan. 2000.

[8] V. Bharghavan, A. Demers, S. Shenker, and L. Zhang, "MACAW: a media access protocol for wireless LANs," in *Proc. SIGCOMM*, 1994.

[9] M. Stojanovic, "Frequency reuse underwater: capacity of an acoustic cellular network," in *Proc. Workshop on Underwater networks (WUWNet)*, 2007, pp. 19–24.

[10] K. Xu, M. Gerla, and S. Bae, "Effectiveness of RTS/CTS handshake in IEEE 802.11 based ad hoc networks," *Ad Hoc Networks*, vol. 1, no. 1, pp. 107–123, 2003.

[11] F. Ye, S. Yi, and B. Sikdar, "Improving Spatial Reuse of IEEE 802.11 Based Ad hoc Networks," in *Proc. GLOBECOM*, 2003, pp. 1013–1017.

[12] T. Rappaport, *Wireless Communications: Principles and Practice*. Prentice Hall, 1996.

[13] D. Pompili, T. Melodia, and I. F. Akyildiz, "Routing algorithms for delay-insensitive and delay-sensitive applications in underwater sensor networks," in *Proc. ACM MobiCom*, 2006, pp. 298–309.

[14] D. Kotz, C. Newport, R. Gray, J. Liu, Y. Yuan, and C. Elliott, "Experimental Evaluation of Wireless Simulation Assumptions," in *Proc. ACM/IEEE MSWiM*, Oct 2004, pp. 78–82.

[15] M. Stojanovic, "On the Relationship Between Capacity and Distance in an Underwater Acoustic Communication Channel," *ACM SIGMOBILE MC2R*, vol. 11, no. 4, pp. 34–43, Oct 2007.

[16] J. Preisig and M. Johnson, "Signal detection for communications in the underwater acoustic environment," *IEEE Journal of Oceanic Engineering*, vol. 26, no. 4, pp. 572–585, 2001.

[17] M.Stojanovic, "Recent Advances in High-Speed Underwater Acoustic Communications," *IEEE Journal of Oceanic Engineering*, vol. 21, no. 2, pp. 125–136, Apr. 1996.

[18] L. Brekhovskikh and Y. Lysanov, *Fundamentals of Ocean Acoustics*, 3rd ed. Springer-Verlag, 2003.

[19] D. Son, B. Krishnamachari, and J. Heidemann, "Experimental study of concurrent transmission in wireless sensor networks," in *Proc. ACM SenSys*, 2006, pp. 237–250.

[20] D. Aguayo, J. Bicket, S. Biswas, G. Judd, and R. Morris, "Link-level measurements from an 802.11b mesh network," in *Proc. ACM SIGCOMM*, 2004, pp. 121–132.

[21] E. Calvo and M. Stojanovic, "Efficient Channel-Estimation-Based Multiuser Detection for Underwater CDMA System," *IEEE J. Oceanic Engineering*, vol. 33, no. 4, Oct 2008.

[22] M. Stojanovic, "Low Complexity OFDM Detector for Underwater Acoustic Channels," in *Proc. IEEE OCEANS Conference*, Sept 2006.

[23] M. Grund, L. Freitag, J. Preisig, and K. Ball, "The PLUSNet Underwater Communications System: Acoustic Telemetry for Undersea Surveillance," in *Proc. IEEE OCEANS Conference*, Sept 2006.

[24] J. Preisig, "Acoustic propagation considerations for underwater acoustic communications network development," *SIGMOBILE Mob. Comput. Commun. Rev.*, vol. 11, no. 4, pp. 2–10, 2007.

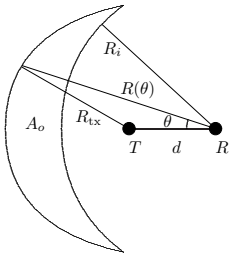

Fig. 10: Area A_o, shown in relation to transmitter T and receiver R. See also Figure Ib.

APPENDIX A
CALCULATION OF SCENARIO IIA EFFECTIVENESS

For the case of Scenario IIa in Figure 1b and Table I, we need to calculate the RTS/CTS effectiveness,

$$E_{\rm RTS/CTS} = \frac{A_{(i \cap \rm RTS/CTS)}}{A_i}, \tag{A-1}$$

introduced in Section II of this paper. The area of the interference region is $A_i = \pi R_i^2$. There are several approaches to calculating $A_{(i \cap \rm RTS/CTS)}$.

Xu et al. [10] and Ye et al. [11] calculate the area of the interference region that is not covered by the RTS/CTS handshake; i.e., the red region in Scenario IIa of Figure 1b. They approximate this region as an angular segment of an annulus. For UANs, Scenario IIb will be common, and that approach leads to a discontinuity in $E_{\rm RTS/CTS}$ at the transition from Scenario IIa to Scenario IIb.

We calculate instead the area of the RTS/CTS handshake that is outside of the interference region; i.e., the green crescent moon at the left side of Scenario IIa in Figure 1. This shape is also illustrated in Figure 10, and it is where $R_{\rm tx} < R_i < R_{\rm tx} + d$. For the idealized geometry in our example, we can calculate $A_{(i \cap \rm RTS/CTS)}$ exactly.

First, we calculate the area covered by the RTS/CTS handshake, $A_{\rm RTS/CTS}$. In Scenario IIa, $R_i < R_{tx} + d$. The area of the region reached by either the RTS packet or the CTS packet is

$$A_{\rm RTS/CTS} = 2\left\{\pi R_{\rm tx}^2 - A_{\rm chord}\right\}. \tag{A-2}$$

Note that the area of a chordal segment of a circle of radius $R_{\rm tx}$ is

$$A_{\rm chord} = R_{\rm tx}^2 \tan^{-1}\left[\sqrt{\left(\frac{R_{\rm tx}}{a}\right)^2 - 1}\right] - a\sqrt{R_{\rm tx}^2 - a^2}, \tag{A-3}$$

where a is the apothem of the chord (see http://mathworld.wolfram.com/Chord.html). The transmitter and receiver are separated by a distance d, and so the sagitta s of the chord is $s = d/2$. Therefore, by definition and substitution,

$$a = R_{\rm tx} - s = R_{\rm tx} - d/2.$$

Now, we calculate $A_{(i \cap \rm RTS/CTS)}$. Let A_o be the area of the RTS/CTS region that is not in the interference region. Therefore, the RTS/CTS effectiveness in Scenario IIa is

$$E_{\rm RTS/CTS} = \frac{A_{(i \cap \rm RTS/CTS)}}{A_i} = \frac{A_{\rm RTS/CTS} - A_o}{A_i} \tag{A-4}$$

What remains is to derive the area A_o, shown in Figure 10

$$A_o = 2 \int_{\theta=0}^{\theta_o} \int_{r=R_i}^{R(\theta)} r \; dr \; d\theta \tag{A-5}$$

where, θ_o is the angle where $R(\theta) = R_i$. By the law of cosines,

$$\theta_o = \cos^{-1} \frac{d^2 + R_i^2 - R_{\text{tx}}^2}{2dR_i} \tag{A-6}$$

Again using the law of cosines, and solving for $R(\theta)$ with the quadratic formula,

$$R(\theta) = d\cos\theta \pm \sqrt{R_{\text{tx}}^2 - d^2 \sin^2\theta}. \tag{A-7}$$

At $\theta = 0$, we can see that we need to take the plus in the $\pm$ for the case of interest. Evaluating the integral for A_o gives

$$\begin{aligned} A_o \quad &= \quad \left(R_{\text{tx}}^2 - R_i^2\right)\theta_o + \frac{d^2}{2}\sin 2\theta_o \\ &\pm \; 2d^2 \left[\frac{u}{2}\sqrt{\left(\frac{R_{\text{tx}}}{d}\right)^2 - u^2} \; + \; \frac{R_{\text{tx}}^2}{2d^2}\sin^{-1}\left(\frac{ud}{R_{\text{tx}}}\right) \right]_{u=0}^{\sin\theta_o} \end{aligned} \tag{A-8}$$

Again, the plus is taken in the $\pm$. Now we have solved for all quantities required to express the RTS/CTS effectiveness for Scenario IIa, following Equation A-4.